

## Propagation of curved stationary flames in tubes

V. V. Bychkov

*Department of Plasma Physics, Umea University, S-90187, Umea, Sweden*

S. M. Golberg and M. A. Liberman

*Department of Physics, Uppsala University, Box 530, S-75121, Uppsala, Sweden*

*P. Kapitsa Institute for Physical Problems, 117 334, Moscow, Russia*

L. E. Eriksson

*Volvo Aero Corporation, Combustor Division, S-461 81, Trollhattan, Sweden*

(Received 12 March 1996; revised manuscript received 18 June 1996)

Dynamics of a curved flame propagating in a tube is investigated by means of two-dimensional numerical simulations. The complete system of hydrodynamical equations including thermal conduction, viscosity, equation of chemical kinetics, and fuel diffusion is solved with the ideally adiabatic and slippery boundary conditions at the tube walls. It is found that only a planar flame can propagate in a narrow tube of width smaller than a half of the cutoff wavelength determined from the linear theory of the hydrodynamic instability of a flame front. In a wider tube, stationary curved flames are obtained, which propagate with the velocities larger than the corresponding velocity of a planar flame. The velocity of a curved flame front is studied as a function of the tube width and the expansion coefficient of the fuel. The influence of viscosity on the velocity of a curved flame front is found to be negligible. The configuration of a curved flame propagating upwards in a gravitational field is also investigated. It is shown that gravity leads to an additional increase of the flame velocity due to the effect of rising bubbles of light burning products. The analytical formulas for the velocity of a flame front are proposed for the cases of both zero and nonzero gravity. [S1063-651X(96)10010-6]

PACS number(s): PACS 47.20.-k, 82.40.Py

### I. INTRODUCTION

The problem of flame dynamics in tubes is one of the most fundamental problems in combustion theory. The theoretical model of the flames in tubes reproduces the main features of a common burning configuration in industrial conditions, such as, for example, the combustion process in gas turbines of aircrafts. Besides, a flame front propagating in a tube represents a typical situation in combustion experiments [1–4]. As was observed experimentally, a flame front in a tube propagates rather seldom as a planar stationary front. Usually the flame acquires a curved shape [3,4] and sometimes transition to a turbulent regime of propagation happens [2], which is accompanied by considerable amplification of the flame velocity. While the observed transition to the turbulent regime may be sometimes accounted for by the interaction of the flow and rough tube walls [2], the curved shape of a flame in tubes is a more common phenomenon. The curved shape of the front appears even for flames propagating in tubes with very smooth and adiabatic walls and it requires another explanation. A flame front may become spontaneously curved because of the hydrodynamic instability first discussed by Landau and Darrieus [1,5,6], which is the main reason for curved shapes of the flame fronts observed in many experiments.

The Landau-Darrieus (LD) instability is inherent to all flames in gaseous mixtures since the instability is related to the gas expansion in exothermal reactions. On the linear stage of the instability the perturbation amplitude grows exponentially with the growth rate  $\sigma$  depending on the perturbation wave number  $k = 2\pi/\lambda$ . For a simple case, when the

evolution of the flame front is not complicated by the thermal-diffusive instability, the instability growth rate has the form

$$\sigma = \Gamma u_f k (1 - k\lambda_c/2\pi), \quad (1)$$

where  $u_f$  is the normal velocity of a planar flame,  $\lambda_c$  is the cutoff wavelength, and the coefficient  $\Gamma$  depends upon the ratio of the fuel density and the density of the burning products  $\Theta = \rho_f/\rho_b > 1$ ,

$$\Gamma = \frac{\Theta}{\Theta + 1} (\sqrt{\Theta + 1 - 1/\Theta} - 1). \quad (2)$$

Perturbations of a wavelength shorter than the cutoff wavelength  $\lambda_c$  are stabilized by thermal conduction. The cutoff wavelength is proportional to the flame thickness  $L$  and it exceeds essentially the flame thickness. Typically for flames in gas mixtures one has  $\lambda_c \approx 20L$ . For the case of the Lewis number equal to unity (equal coefficients of thermal diffusivity and fuel diffusion) and a large activation energy of the reaction,  $E/RT_b \gg 1$  ( $T_b$  being the temperature of the burnt matter) the cutoff wavelength may be estimated by the analytical formula [7–10]

$$\lambda_c = \frac{\pi L (\Theta - 1)}{\Gamma \sqrt{\Theta + 1 - 1/\Theta}} \left( 1 + \Theta \ln \Theta \frac{\Theta + 1 + 2\Gamma}{(\Theta - 1)^2} \right). \quad (3)$$

For the case of moderate values of the activation energy  $E/RT_b \geq 1$  the cutoff wavelength can be calculated using the method proposed in [10].

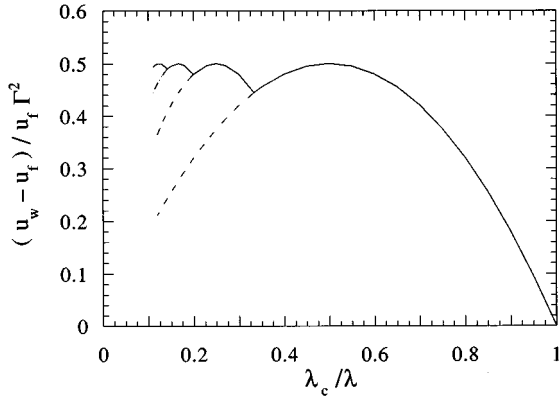


FIG. 1. The scaled velocity of a stationary cellular flame vs the inverse cell size  $\lambda_c/\lambda$  obtained in the limit of a small expansion coefficient  $\Theta - 1 \ll 1$ . The dashed lines of the curve correspond to the unstable solutions.

Development of the LD instability causes an increase of the flame front surface which in turn leads to the acceleration of the flame. However, there is a mechanism of nonlinear stabilization preventing infinite acceleration of flames in tubes, as was pointed out in [11]. If a flame propagates in a tube of moderate width comparable to the cutoff wavelength, then the growth of perturbations causes formation of cusps at the flame front and leads to the configuration of the stationary curved flames observed experimentally in [3,4]. Such curved flames propagate with higher velocity compared to the planar flames. As is expected, in tubes of moderate width a curved flame front consists of a few cells separated by cusps [11,12]. In much wider tubes such a configuration cannot be stable any more. If the cell size is large enough in comparison with the cutoff wavelength, then the cellular flame in turn becomes unstable against the LD instability of a small scale. As a result of this secondary instability a fine structure arises on large cells [13,14]. Further development of the secondary LD instability is possible if the largest instability length scale exceeds the cutoff wavelength by many orders of magnitude. In this case a fractal structure develops at the flame front which implies many cascades of small cells imposed on large cells [15–18].

Up to now there was mostly qualitative understanding of the nonlinear stage of the LD instability. Theoretical analysis of the nonlinear stage of LD instability has been restricted at most by the investigation of flame behavior in the limit of the small expansion coefficient,  $\Theta - 1 \ll 1$  [12,14,16,17,19]. Particularly in the limit of a small expansion coefficient the model equation for a curved flame front has been derived in [12] and the analytical solution of this equation has been obtained in [19]. It follows from the analytical solution [19] that velocity of a stationary curved flame front with periodic cellular structure depends on the cell size in a way shown in Fig. 1. The important feature of the dependence is existence of a maximal possible velocity of a stationary cellular flame front. For example, this maximum is achieved for the period of the cellular structure  $\lambda_m = 2\lambda_c$  which results from the fastest growing perturbations on the linear stage of the instability growth. Except for the study of the specific limit of small expansion coefficients only semiquantitative analytic estimates of the velocity of a curved flame front are available [11,13].

The purpose of the present paper is to investigate the nonlinear stage of the LD instability by means of two-dimensional (2D) numerical simulations of the complete system of hydrodynamical equations and equations of chemical kinetics. There have been several papers devoted to 2D numerical simulations of LD instability of a flame front in a laboratory or astrophysical environment, e.g., [20–23]. Particularly, the linear stage of the LD instability of a planar flame has been studied thoroughly in [22] by means of 2D simulations. However, when it comes to the nonlinear stage of the LD instability, all these papers resulted only in qualitative descriptions of the simulated flows. Therefore careful quantitative investigation of the dynamics of curved flames is necessary.

In the present paper we study propagation of a curved flame front in a tube with ideally adiabatic and slip walls. Such a configuration corresponds to the development of a periodic cellular structure at a flame front as well, since the ideal walls may be considered as the symmetry axes. In the present paper we restrict ourselves to the case of tubes of a moderate width compared to the cutoff wavelength. By this restriction we concentrate our study on the development and propagation of stationary cellular flames. One of the goals of the present paper is to investigate the maximal velocity of a stationary curved flame in tubes. We also consider the configuration of curved upward propagating flames and study the effect of gravity on flame dynamics. Problems of stability of a cellular flame and development of a fractal structure will be addressed in the forthcoming papers.

The paper is organized as follows. In Sec. II a basic set of the equations is introduced and the problem of a flame propagating in a tube is formulated. Section III contains a brief description of the 2D numerical scheme. In Sec. IV results of several tests of the numerical code for the well known analytical solutions of flame dynamics are presented. We found that the Zel'dovich-Frank-Kamenetski solution for a planar stationary flame front [1] and the linear stage of the LD instability are reproduced with a very good accuracy. The obtained results on the dynamics of curved flames in tubes and discussion of the results are presented in Sec. V. In Sec. VI we present results of the numerical simulations of upward propagation of slow flames in a tube. The analytical formulas are obtained for the velocity of a curved stationary flame for both cases of zero and nonzero gravity. We conclude in Sec. VII.

## II. BASIC EQUATIONS

We solve, numerically, equations of hydrodynamics and chemical kinetic. For the sake of simplicity a single irreversible reaction is admitted, so that the governing equations are the following:

$$\frac{\partial}{\partial t} \rho + \frac{\partial}{\partial x_i} (\rho u_i) = 0, \quad (4)$$

$$\frac{\partial}{\partial t} (\rho u_i) + \frac{\partial}{\partial x_j} (\rho u_i u_j) + \delta_{ij} P - \tau_{ij} = 0, \quad (5)$$

$$\frac{\partial}{\partial t} \left( \rho e + \frac{1}{2} \rho u_i u_j \right) + \frac{\partial}{\partial x_i} \left( \rho u_i h + \frac{1}{2} \rho u_i u_j u_j - q_i - u_j \tau_{ij} \right) = 0, \quad (6)$$

$$\frac{\partial}{\partial t} (\rho Y) + \frac{\partial}{\partial x_i} \left( \rho u_i Y - \frac{\mu}{Sc} \frac{\partial Y}{\partial x_i} \right) = - \frac{\rho Y}{\tau_R} \exp(-E/RT), \quad (7)$$

where  $Y$  is the fuel fraction,  $e = QY + C_V T$  is the internal energy,  $h = QY + C_P T$  is the enthalpy,  $Q$  is the energy release in the reaction. The specific heats  $C_V$ ,  $C_P$  are assumed to be constant and unaffected by reaction. We consider a reaction of the first order; the temperature dependence of the reaction rate is given by the Arrhenius law with the activation energy  $E$  and the constant of time dimension  $\tau_R$ . The stress tensor and the energy diffusion vector are given by the formulas

$$\tau_{ij} = \mu \frac{\partial u_i}{\partial x_j} + \mu \frac{\partial u_j}{\partial x_i} - \frac{2}{3} \mu \delta_{ij} \frac{\partial u_k}{\partial x_k}, \quad (8)$$

$$q_i = C_P \frac{\mu}{Pr} \frac{\partial T}{\partial x_i} + Q \frac{\mu}{Sc} \frac{\partial Y}{\partial x_i}, \quad (9)$$

where  $Pr$  is the Prandtl number and  $Sc$  is the Schmidt number (their ratio gives the Lewis number  $Le = Pr/Sc$ ). We take the gas mixture under consideration to be a perfect gas of molecular weight  $m$  unaffected by reaction, so that the equation of state is

$$P = \frac{R}{m} \rho T, \quad (10)$$

where  $R \approx 8.3$  J/(deg mol) is a gas constant.

The flame is assumed to propagate in a tube of width  $D$  with ideally adiabatic and slip conditions at the walls

$$u_x = 0, \quad u_z \neq 0, \quad \frac{\partial T}{\partial x} = 0, \quad \text{at } x = 0, D. \quad (11)$$

We choose the axis  $z$  directed along the tube wall and the axis  $x$  perpendicular to the walls. An infinite length of the tube is assumed which is achieved in simulations by an appropriate choice of the computational intervals.

The initial temperature of the fuel is  $T = 300$  K and the pressure is  $P = 10^5$  Pa. The viscosity coefficient of the fuel is  $\mu = 1.7 \times 10^{-3}$  N s/m<sup>2</sup>, with the molecular weight being  $m = 2.9 \times 10^{-3}$  kg/mol and the specific heat  $C_P = 7R/3m$ . The velocity of a planar stationary flame  $u_f$  is determined by the chosen values of the chemical parameters of the fuel  $E$ ,  $Q$ ,  $\tau_R$ . We are interested in the dynamics of the flames with the velocities  $u_f$  much less than the sound speed  $c_s$ . For this reason we adjusted parameters of the fuel in such a way that the Mach number is  $M = u_f/c_s = 0.01 \ll 1$ .

To investigate the development of the LD instability without influence of the thermal-diffusion instability we keep always  $Le = Pr/Sc = 1$ . In most of the calculations we take  $Pr = Sc = 0.3$ , still the influence of viscosity on the dynamics of a curved flame (different Prandtl numbers) is also investigated. The main parameters of the simulations are the tube width and the expansion coefficient defined as the ratio of

densities of the fuel and the burnt gas:  $\Theta = \rho_f/\rho_b$ . For the case of subsonic flames the flow is isobaric within the accuracy  $M^2 \ll 1$ , so that the expansion coefficient is equal to the ratio of temperatures of the fuel and the burning products  $\Theta = T_b/T_f$ . For this reason the expansion coefficient may be governed by alteration of the energy release in the reaction  $\Theta = 1 + Q/C_P T_f$ . For given chemical parameters of the fuel the expected velocity of a planar stationary flame has been calculated by the method used in [10]. When the velocity of a planar flame is known, the thickness of the flame front can be estimated by the formula

$$L = \frac{\mu}{Pr \rho_f u_f}. \quad (12)$$

Another parameter of our simulations is the activation energy of the reaction. For most of the laboratory flames the activation energy is quite large  $E/RT_b = 10 - 20$ . However, a large activation energy implies a narrow zone of chemical reactions  $L_R$  compared to the total flame thickness  $L_R \approx LRT_b/E \ll L$ , which in turn requires the fine gridding to resolve the reaction zone. By this reason we choose moderate values of the activation energy to spread the reaction zone over 7–10 computational cells. For the flames with expansion coefficients  $\Theta = 5, 7, 10$  we chose the activation energy  $E/RT_b = 5$ . For the flames with smaller expansion coefficients it is necessary to take larger values of activation energy to avoid the undesirable effect of spontaneous reaction ahead of the flame front [1]. For example, we take  $E/RT_b = 7$  for the flame with the expansion coefficient  $\Theta = 3$ . Luckily, development of the LD instability for the case of the Lewis number equal to unity is not sensitive to the value of the activation energy [1,10]. That's why the choice of moderate values of the activation energy makes no restrictions on the obtained physical results.

### III. THE NUMERICAL SCHEME

We have performed the numerical simulations using a 2D hydrodynamic Eulerian code which accounts for chemical reactions. The code is based on the cell-centered finite-volume scheme. This numerical method appears to be quite effective when used to model different kinds of complex hydrodynamic flows [20,24–27].

To construct the cell-centered finite-volume scheme any equation of the system (4)–(7) should be rewritten in the form of the conservation law

$$\frac{\partial G}{\partial t} + \frac{\partial E_G}{\partial x} + \frac{\partial F_G}{\partial z} = H_G, \quad (13)$$

where  $G$  stands for any of the variables  $\rho$ ,  $\rho u_x$ ,  $\rho u_z$ ,  $\rho e + (1/2)\rho(u_x^2 + u_z^2)$ ,  $\rho Y$ ;  $E_G$ , and  $F_G$  stand for the corresponding fluxes and  $H_G$  gives a source term. The cell-centered finite-volume spatial discretization is obtained by integrating the conservation law in the form (13) over a given grid cell. As an example, we present here the result of integration for an interior cell with indices  $i, j$ . We assume that purely integer indices  $(i, j)$  denote a grid cell, mixed

fractional-integer indices denote the cell walls and purely fractional indices denote the grid nodes. Within this notation we have

$$\begin{aligned} \frac{d}{dt} \bar{G}_{i,j} + (E_G)_{i+1/2,j} - (E_G)_{i-1/2,j} + (F_G)_{i,j+1/2} - (F_G)_{i,j-1/2} \\ = (\bar{H}_G)_{i,j}, \end{aligned} \quad (14)$$

where

$$\begin{aligned} \bar{G}_{i,j} &= \frac{1}{\alpha_{i,j}} \int_{\Omega_{i,j}} G dS, \quad (\bar{H}_G)_{i,j} = \frac{1}{\alpha_{i,j}} \int_{\Omega_{i,j}} H dS, \\ \alpha_{i,j} &= \int_{\Omega_{i,j}} dS, \quad (E_G)_{i+1/2,j} = \int_{B_{i+1/2,j}} (E_G n_x + F_G n_z) dl, \\ (F_G)_{i,j+1/2} &= \int_{B_{i,j+1/2}} (E_G n_x + F_G n_z) dl. \end{aligned} \quad (15)$$

$\Omega_{i,j}$  is the grid cell  $(i,j)$ ;  $B_{i+1/2,j}$  and  $B_{i,j+1/2}$  are the cell walls between the current cell  $(i,j)$  and the cells  $(i+1,j)$  and  $(i,j+1)$ , respectively;  $\mathbf{n} = (n_x, n_z)$  is the normal to the corresponding cell wall.

By choosing the cell averages of the state vector  $\bar{G}_{i,j}$  as the unknowns of the discretized problem and introducing approximations of the fluxes  $(\bar{E}_G)_{i+1/2,j}$  and  $(\bar{F}_G)_{i,j+1/2}$  and the cell averaged source vector  $(\bar{H}_G)_{i,j+1/2}$  in terms of these unknowns, we arrive at the final spatial discretization of (13).

A key feature of the cell-centered finite-volume discretization of (13) given by (14) is the numerical approximation of the fluxes  $(\bar{E}_G)_{i+1/2,j}$  and  $(\bar{F}_G)_{i,j+1/2}$  in terms of the cell averages  $\bar{G}_{i,j}$ . The usual approach is to treat the convective flux approximations and the diffusive flux approximations separately because of the different nature of these fluxes. For the convective fluxes we use a characteristic-upwind flux scheme [28] in which the propagation directions of the various characteristic variables control a user-given degree of upwinding. Here it turns out to be advantageous to work with the hydrodynamical variables  $\rho$ ,  $u_x$ ,  $u_z$ ,  $P$ ,  $Y$  instead of the conservative variables in the state vector  $\bar{G}_{i,j}$ . The numerical errors introduced by using this approximation are of the second order in the grid spacing assuming a smooth solution. For problems where all spatial scales are adequately resolved in the computational grid, an extremely small amount of upwinding may be used giving an almost centered scheme with minimal numerical dissipation and dispersion.

Boundary conditions at the tube walls (11) are approximated in a traditional manner providing an approximation of the second order in the grid spacing. At the same time one should pay special attention to the boundary conditions imposed at the ends of the tube. Though we are interested in flame dynamics in a tube of infinite length, a finite computational domain requires the boundary conditions to be imposed at finite displacements  $z = \pm Z_\infty$  instead of  $z = \pm \infty$ . Therefore the value of  $Z_\infty$  must be chosen large enough so that the flow at  $z = \pm Z_\infty$  can be treated as uniform. In our modeling we use an Eulerian resting grid, therefore the unburnt matter flows into the calculation domain at  $z = -Z_\infty$  and the burnt matter flows out of the domain at  $z = +Z_\infty$ .

Simulations start from the initial state which corresponds to the planar flame front in the vicinity of  $z=0$ . The size of the fine mesh in the vicinity of  $z=0$  is adjusted to the structure of the flame front and the energy release zone. To maintain the flame front near  $z=0$  on the fine mesh adjusted to the flame thickness we impose the following boundary conditions on the incoming flow of the unburnt matter at  $z = -Z_\infty$ :

$$T = T_f, \quad \rho = \rho_f, \quad u_z = u_f, \quad u_x = 0, \quad Y = 1. \quad (16)$$

Similar boundary conditions for the outgoing uniform flow of the burnt matter ( $Y=0$ ) follow from the conservation laws of mass, momentum, and energy. These conditions are imposed at  $z = +Z_\infty$ .

To eliminate the influence of the particular value of  $Z_\infty$  on the results of numerical simulations this value should be large in comparison with any other length scale. The characteristic length scales of the problem can be estimated from the linear stability analysis [7, 24]. They are: the flame thickness  $L$ , the hydrodynamical length scale, which is about the tube width  $D$ , and the length scale of vorticity dissipation behind the flame front

$$L_\mu = L \left[ \sqrt{\frac{1}{4\text{Pr}^2} + (\pi L/D)^2} + \frac{\pi \Gamma L}{\Theta \text{Pr} D} - \frac{1}{2\text{Pr}} \right]^{-1}. \quad (17)$$

Another restriction on the tube length comes from the requirement to eliminate the chemical-acoustic instability. This instability arises as a result of the resonant interaction of the acoustic oscillations in a tube of finite length and the energy release in the reaction. It was pointed out in [29] that the chemical-acoustic coupling does not lead to the instability if a characteristic acoustic time  $Z_\infty/c_s$  is large compared to the characteristic chemical time scale  $L/u_f$ . Therefore in order to suppress the instability the tube length must be chosen considerably larger than  $L/M$ . In our calculations we use  $Z_\infty = 500L$  to satisfy all the restrictions mentioned above.

We use a rectangular grid with the grid walls parallel to the coordinate axis. When choosing the grid step we take into account the characteristic scales of the flow under consideration. The characteristic length scale along the  $x$  axis is the distance  $D$  between the walls. Therefore along the  $x$  axis the grid is uniform with the grid step  $d_x = D/N_x$ , with  $N_x = 16$  for  $D < \lambda_m/2$  and  $N_x = 32$  for  $D > \lambda_m/2$  (the last case corresponds to the situation when perturbations with the wavelengths  $\lambda = 2D$  and  $\lambda = D$  are both unstable). To perform all the calculations in a reasonable time we use a non-uniform grid along the  $z$  axis: the space step of the grid is constant (about  $L/10$ ) in the area  $-6L < z < 6L$ , where the flame front is maintained and the grid step gradually grows outside the area with 18% change in size between adjacent cells, as recommended in [30].

To avoid spurious reflections from the artificial boundaries  $z = \pm Z_\infty$  the boundary conditions were used in the form of a far-field dumping operator, analogous to [31]. The boundary conditions are based on the characteristic variables and the characteristic speeds normal to the boundary. A local linearization of the governing equations in the form (13) was done to obtain a linear advection problem normal to the boundaries at  $z = \pm Z_\infty$ :

$$\frac{\partial G}{\partial t} + J_F \frac{\partial G}{\partial z} = 0, \quad (18)$$

where  $J_F = \partial F_G / \partial G$  is the Jacobian of the flux vector  $F_G$  with respect to the solution vector  $G$ . As is seen, the boundary conditions (18) include only the direction normal to the boundary, which means that only disturbances in the form of a planar wave traveling in the direction normal to the boundary are present. Equation (18) may be transformed into a set of scalar equations in the form

$$\frac{\partial W_n}{\partial t} + \lambda_{J,n} \frac{\partial W_n}{\partial z} = 0, \quad (19)$$

where  $\lambda_{J,n}$  is the  $n$  th eigenvalue of the matrix  $J_F$ ,  $W_n$  is the  $n$  th component of the vector  $W = T_J^{-1} G$  and  $T_J$  is the diagonalizing matrix:  $T_J^{-1} J_F T_J = \text{diag}(\lambda_{J,1}, \lambda_{J,2}, \dots)$ . Equation (19) expresses the transfer of each characteristic variable  $W_n$  by the flow with the characteristic speed  $\lambda_{J,n}$ . Then the sign of the characteristic speed determines if the corresponding characteristic variable is traveling out of the calculation domain or into the domain. The principle we used serves to impose the boundary conditions (16) only on those characteristic variables that travel into the domain and to extrapolate (from the interior) those that travel out of the domain. This way of treating the boundary conditions at  $z = \pm Z_\infty$  results in complete suppression of spurious reflected sound waves, which present in a numerical modeling if the special precautions are not applied.

#### IV. SIMULATIONS OF A PLANAR FLAME AND THE LINEAR STAGE OF THE LANDAU-DARRIEUS INSTABILITY

The numerical code has been tested on well known solutions of the problems of flame dynamics and stability. Particularly, it was verified whether the numerical simulation reproduces properly propagation of a planar stationary flame front and the linear stage of the LD instability.

To study propagation of a planar flame the analytical solution obtained by Zel'dovich and Frank-Kamenetskii [1] was chosen as an initial state. In the coordinate system comoving with the flame front the solution can be written in the form

$$T = \begin{cases} T_f + T_f(\Theta - 1)\exp(z/L), & z < 0 \\ T = \Theta T_f, & z > 0 \end{cases} \quad (20)$$

$$u_z/u_f = \rho_f/\rho = T/T_f, \quad Y = \frac{\Theta - T/T_f}{\Theta - 1}, \quad (21)$$

$$P = \begin{cases} P_f + (\frac{4}{3}\text{Pr} - 1)(\Theta - 1)\rho_f u_f^2 \exp(z/L), & z < 0 \\ P_f - (\Theta - 1)\rho_f u_f^2, & z > 0. \end{cases} \quad (22)$$

The starting estimate for the velocity of the planar stationary flame is given by the formula

$$u_{ZF} = \left( \frac{\mu}{\text{Pr}\rho_f\tau_R\Lambda} \right)^{1/2}, \quad (23)$$

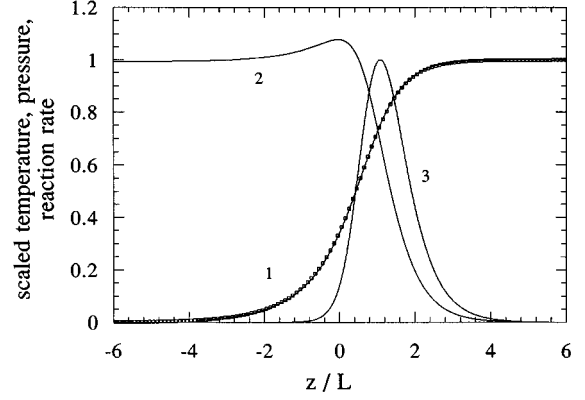


FIG. 2. Profiles of the hydrodynamical variables for a planar flame front with the expansion coefficient  $\Theta = 5$ . Curve 1 corresponds to the scaled temperature  $(T - T_f)/(T_b - T_f)$ , the solid line gives the solution of the eigenvalue problem [10], and the markers show the result of numerical simulation (mesh points); curve 2 corresponds to the scaled pressure  $(P - P_b)/(P_f - P_b)$ ; curve 3 corresponds to the reaction rate scaled by its maximal value.

where

$$\Lambda = \frac{E^2(\Theta - 1)^2}{2R^2T_f^2\Theta^3} \exp(E/\Theta RT_f). \quad (24)$$

The important feature of the analytical solution is the pressure difference between the ends of the tube  $[P] = (\Theta - 1)\rho_f u_f^2$  given by Eq. (22). This pressure difference was taken as initial boundary conditions at the ends of the tube. After a time interval comparable to the time necessary for a sound wave to propagate from one end of the tube to another, the stationary flow was formed. The flow corresponded to a planar flame front propagating with a constant velocity  $u_f$  respective to the fuel. The real velocity of the flame  $u_f$  was slightly different from the estimate  $u_{ZF}$  given by Eq.(23), and therefore in the laboratory reference frame the stationary flame front moved with a small speed  $u_f - u_{ZF}$ . For this reason the pressure difference  $[P]$  was adjusted until a steady front at rest in the laboratory reference frame (relative to the grid) was obtained in simulations. In this reference frame the fresh fuel flows towards the flame front with the velocity  $u_f$ . Inside the flame front the fuel burns and the gas temperature increases to the final value. The burnt products are drifted away from the flame front in the downstream flow. The resulting profiles of temperature, pressure, and reaction rate for the stationary flame front with the expansion coefficient  $\Theta = 5$  are presented in Fig. 2. A very good agreement of the simulations and the solution of the eigenvalue problem for a planar flame front [10] is seen in Fig. 2: curve 1 shows solution of the eigenvalue problem for the temperature of a planar flame front [10], the markers give the result of the numerical simulation. The pressure jump is seen on curve 2 for the scaled pressure. At the same time we would like to emphasize that the absolute value of the pressure jump is negligible  $[P]/P_f = 5.3 \times 10^{-4}$ , which is about  $M^2$ .

Another test of the numerical code was simulation of the linear stage of the LD instability for a planar flame front. The velocity component  $u_z$  of the obtained stationary solution for a planar flame front was perturbed as  $u_z(z) \rightarrow u_z(z) + \tilde{u}_0(z, x)$ , where

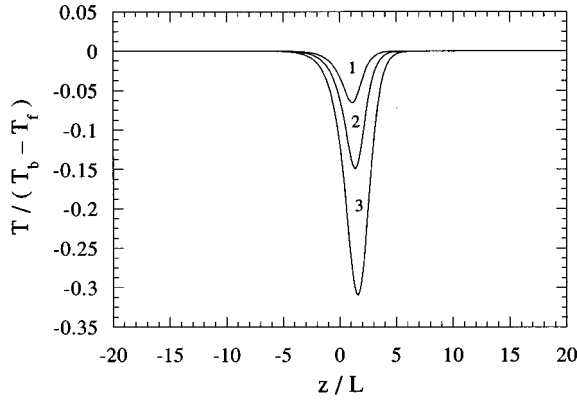


FIG. 3. Time evolution of the temperature perturbations  $\tilde{T}/(T_b - T_f)$  of a flame front with the expansion coefficient  $\Theta=5$  in a tube of width  $D=\lambda_c$ . The curves 1, 2, 3 correspond to the time  $u_f(t-t_0)/L=0;9.3;18.6$ , respectively.

$$\tilde{u}_0(z,x) = u_z(z)A_0 \cos(\pi x/D) \exp\left(-\frac{\pi^2(z-z_0)^2}{D^2}\right). \quad (25)$$

The initial dimensionless perturbation amplitude was taken  $A_0=10^{-4}$  and the maximum of the initial perturbations was chosen at the point  $z_0$  in the reaction zone, where temperature differs slightly from the final value  $T=T_b(1-RT_b/E)$ . The velocity perturbation induced perturbations in density, temperature, pressure, and concentration. When the amplitude of the velocity perturbation became ten times larger than the initial amplitude  $A_0$  (at the time instant  $t_0$ ) all perturbations developed in accordance with the eigenmode of the solution of the eigenvalue problem [10]. The time evolution of temperature perturbations for a flame front with the expansion coefficient  $\Theta=5$  in a tube of width  $D=\lambda_c$  is shown in Fig. 3. All perturbations have a well pronounced maximum. The temperature perturbations as well as density and concentration perturbations are localized around the flame front on the length scale of about flame thickness  $L$ . The perturbations of velocity and pressure are spread on the hydrodynamical length scales of about tube width  $D$  and larger, as was discussed in the preceding section. The amplitudes of all perturbations were measured by the ratio of the perturbation maximum to the value of this maximum at the time instant  $t_0$ . For example, the amplitude of temperature perturbations was measured as

$$A_T(t) = \frac{\max_z[\tilde{T}(z,t)\cos(\pi x/D)]}{\max_z[\tilde{T}(z,t_0)\cos(\pi x/D)]}. \quad (26)$$

In agreement with the linear theory all perturbations grew exponentially with the same instability growth rate, so that the equality

$$\ln A_T(t) = \ln A_\rho(t) = \ln A_{u_z}(t) = \ln A_{u_x}(t) = \sigma(t-t_0), \quad (27)$$

$$\sigma = \text{const}$$

was fulfilled with 0.5% accuracy. The instability growth rate  $\sigma$  obtained from (27) is in good agreement with the predic-

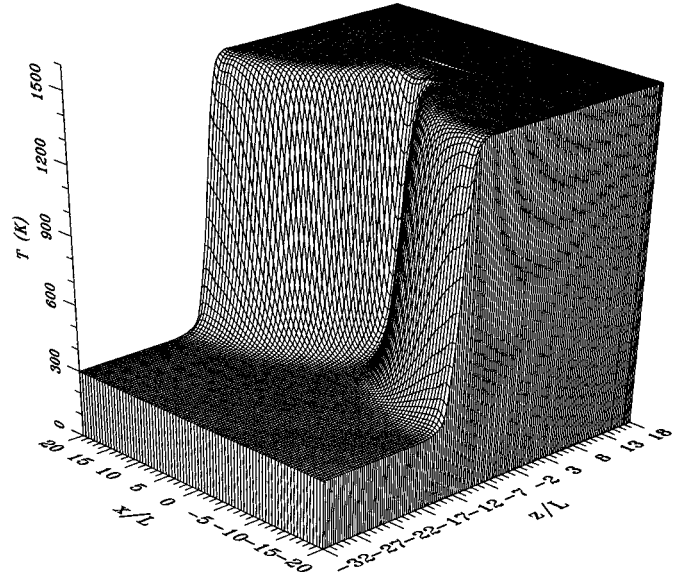


FIG. 4. The temperature of the cellular flame front with the expansion coefficient  $\Theta=5$  propagating in a tube of width  $D=2\lambda_c$ .

tions of the linear theory [10]. Particularly for the flame front with the expansion coefficient  $\Theta=5$  and the tube width  $D=\lambda_c$  ( $\lambda_c$  is the cutoff wavelength calculated by solution of the eigenvalue problem [10]) the theoretically predicted growth rate is  $\sigma=0.088u_f/L$ , while the numerical simulation gives the growth rate  $\sigma=0.084u_f/L$ . The perturbations grow in agreement with the linear theory until the dimensionless amplitude becomes  $A_T \approx 10$ . At this time the dimensional amplitudes of perturbations are approximately hundred times smaller than the corresponding values of the unperturbed flow. On the later stage the nonlinear effects on the growth of perturbations become noticeable.

## V. CURVED FLAME PROPAGATION IN THE CASE OF ZERO GRAVITY

Dynamics of a curved flame front have been investigated for different widths of the tube and different values of the expansion coefficient. One of the main parameters that affect the propagation regime of a curved flame in a tube is the ratio of the tube width and the cutoff wavelength  $\lambda_c$ . The exact values of the cutoff wavelength are calculated by the method used in [10]. Because of the ideal boundary conditions at the walls Eq. (11) the tube width  $D$  determines a half of the largest possible wavelength of permitted perturbations  $\lambda=2D/n$ ,  $n=1,2,3$ , etc. For perturbations of a wavelength shorter than the cutoff wavelength development of the LD instability is suppressed by thermal conduction. If a tube is sufficiently narrow  $D<\lambda_c/2$ , then all permitted perturbations belong to the stable part of the dispersion relation Eq.(1). In agreement with the theory the numerical simulation demonstrates that flame evolution in narrow tubes  $D<\lambda_c/2$  always leads to a planar flame front. Even in a case of a rather large amplitude of imposed initial perturbations ( $A_0=0.1$ ) the flame front returned to the planar configuration.

In wider tubes,  $D>\lambda_c/2$ , the hydrodynamic instability de-

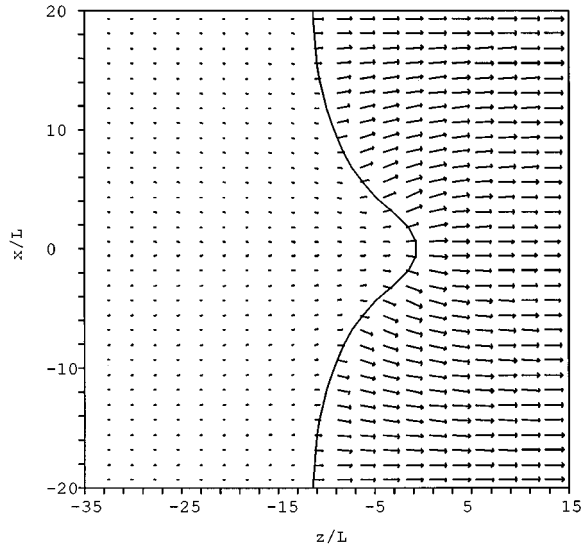


FIG. 5. The velocity field for a curved flame front with the expansion coefficient  $\Theta=5$  obtained in numerical simulations for a tube width  $D=2\lambda_c$ . The solid line shows the isotherm  $T=400$  K.

velops and results in a stationary curved shape of a flame front. We found that the first harmonic with the wavelength  $\lambda=D$  induces the growth of harmonics with smaller wavelengths  $\lambda=D/2, D/3$ , etc., due to the nonlinear interaction. The amplitudes of all harmonics grow with time until the final amplitudes corresponding to the stationary curved flame front to be achieved. The resulting shape of the stationary curved flame with the expansion coefficient  $\Theta=5$  is shown in Fig. 4. The numerical simulation confirms the qualitative idea of a curved flame front composed of cells [11], which are separated by cusps pointing to the products of burning. However, unlike the qualitative picture obtained in [11,13] on the basis of the model of an infinitely thin flame front, the cusps in Fig. 4 are smoothed by thermal conduction. The velocity field for the curved flame front with the expansion coefficient  $\Theta=5$  is shown in Fig. 5. An interesting phenomenon one can observe is the generation of vorticity  $\omega = \partial u_x / \partial z - \partial u_z / \partial x$  behind the curved flame front (Fig. 6) which is an important feature of the flame dynamics [1]. Vorticity is produced, at most, close to the cusp points of the flame front, while near the humps the flow remains irrotational. The produced vorticity is drifted by the downstream flow and dissipates because of the viscous effects, so that the flow at the exit of the tube is uniform again.

A curved flame front propagates with the velocity  $u_w$  larger than the corresponding velocity of a planar flame front. The velocity of a curved flame was calculated as

$$u_w = \frac{\rho_f u_1 - \rho_b u_2}{\rho_f - \rho_b}, \quad (28)$$

where  $u_1$  is the fuel velocity at the entrance of the tube and  $u_2$  is the velocity of the products of burning at the tube exit. Dependence of the velocity of a curved flame front on the tube width was investigated for different expansion coefficients. For any expansion coefficient  $\Theta$  the calculated velocities of the curved flames in tubes of different widths  $D$  with a very good accuracy may be described by the formula

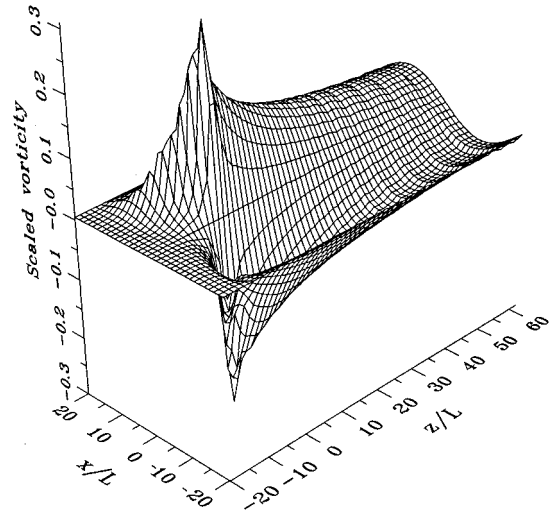


FIG. 6. The scaled vorticity  $\omega L / u_f$  behind the curved flame front with the expansion coefficient  $\Theta=5$  propagating in a tube of width  $D=2\lambda_c$ .

$$u_w = u_f + 4[U_m(\Theta) - u_f] \frac{\lambda_c}{2D} \left(1 - \frac{\lambda_c}{2D}\right), \quad (29)$$

where  $U_m(\Theta)$  is the maximal velocity depending upon the expansion coefficient. The calculated velocity of a curved flame is plotted in Fig. 7 versus the inverse tube width for the expansion coefficients  $\Theta=5$  (curve 1) and  $\Theta=3$  (curve 2). The solid lines correspond to the formula Eq. (29) with the coefficients  $U_m$  and  $\lambda_c$  providing the best fit of the numerical results. The cutoff wavelengths  $\lambda_c$  calculated in such a way agree well with the cutoff wavelengths found from the solution of the eigenvalue problem [10]. The obtained dependence of the velocity of a curved flame upon the tube width is similar to the first parabola piece in Fig. 1 representing the analytical solution for the velocity of a stationary cellular flame front with a small expansion coefficient  $\Theta-1 \ll 1$ . The velocity maximum  $u_w = U_m(\Theta)$  is achieved for the tube width  $D = \lambda_c$ . Because of the ideal boundary conditions Eq.

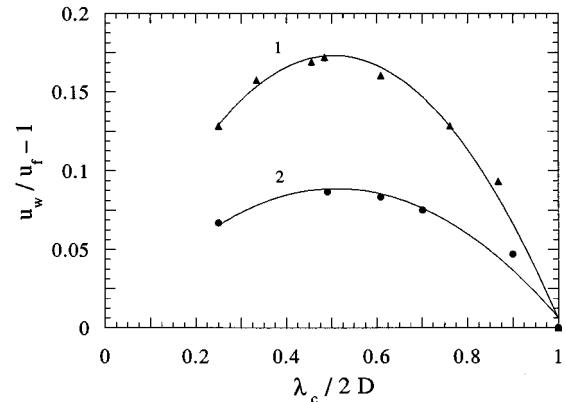


FIG. 7. The scaled velocity of a curved stationary flame  $u_w / u_f - 1$  with the expansion coefficients  $\Theta=5$  (curve 1) and  $\Theta=3$  (curve 2) vs the inverse tube width  $\lambda_c / 2D$ . The markers correspond to the results of the numerical simulation; the solid lines give the best analytical fit in the form of Eq. (29).

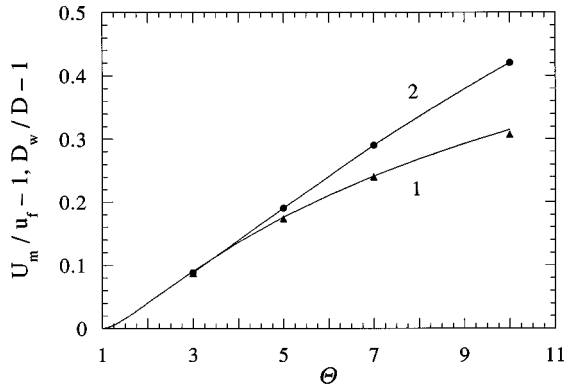


FIG. 8. Increase of the flame velocity and the length of the front vs the expansion coefficient  $\Theta$  for curved flames propagating in tubes of the width  $D = \lambda_c$ . Filled triangles show the velocity increase  $U_m/u_f - 1$  obtained in the numerical simulations, curve 1 presents the analytical formula Eq. (30). Curve 2 and filled circles show the increase of the length of the curved flames  $D_w/D - 1$ .

(11) in this case the curved stationary flame results from the development of the perturbation mode with the wavelength  $\lambda_m = 2\lambda_c$ , which is the fastest mode on the linear stage of the instability according to Eq. (1).

One of the main characteristics of the dynamics of curved flames is the dependence of the maximal velocity  $U_m$  on the expansion coefficient  $U_m = U_m(\Theta)$ . The maximal velocity of a curved stationary flame was calculated for the expansion coefficients  $\Theta = 3, 5, 7, 10$ . Results of the numerical simulations are presented in Fig. 8, where the triangles show the scaled maximal velocity  $U_m/u_f - 1$  obtained in the simulations as a function of the expansion coefficient  $\Theta$ . The maximal velocity of a curved flame may be approximated with a good accuracy by the analytical formula

$$U_m/u_f = 1 + \frac{1}{2} \frac{\Gamma^2}{\Theta} \left( 1 + \frac{\Gamma^2}{\Theta} \right), \quad (30)$$

where the coefficient  $\Gamma$  appears in the linear theory of the LD instability Eq. (2). Curve 1 in Fig. 8 shows the velocity of a curved flame front according to Eq. (30). In the limit of a small expansion coefficient  $\Theta - 1 \ll 1$  the velocity of a curved flame Eq. (30) coincides with the analytical theory [12,19]. The main tendency of the calculated flame velocities is that the larger the expansion coefficient, the larger the velocity of a curved flame. This tendency is physically reasonable since larger expansion coefficients imply a stronger hydrodynamic instability Eq. (1). Besides, the larger the expansion coefficient the more the curvature of the flame front and the larger the length of the curved front. The increase of the surface of a curved flame front  $D_w/D$  is shown in Fig. 8 (curve 2 and the filled circles). Here

$$D_w = \int_0^D \sqrt{1 + \left( \frac{dZ_T}{dx} \right)^2} dx \quad (31)$$

and  $Z_T(x)$  corresponds to the isotherm  $T = 0.8T_b$ . As is seen from Fig. 8, the dependence of the flame velocity and the length of the flame front upon the expansion coefficient  $\Theta$  are the same within the accuracy of simulations until

$\Theta < 5$ . For larger expansion coefficients there is no quantitative agreement any more between the increase of the flame front velocity and the increase of the surface of the flame front, still a very good correlation remains.

It is worth comparing the obtained velocities with the analytical estimates [13], where velocity of a curved stationary flame of zero thickness has been considered. The direct comparison of these results is difficult, since an infinitely thin stationary flame front is inherently unstable and cannot be observed in numerical simulations. However, it can be seen from Fig. 1 that in the limit of small expansion coefficients the velocity of an infinitely thin stationary flame ( $\lambda_c/\lambda \rightarrow 0$ ) coincides with the local velocity maximum of the first parabola piece at  $\lambda = 2\lambda_c$ . If we assume that this feature holds for any expansion coefficient, then comparison of the obtained results and the results of Ref. [13] becomes straightforward. The comparison shows that the increase of the flame velocity due to the curved shape of the front has been overestimated in Ref. [13]. The difference between the estimate of [13] and the results obtained in numerical simulations is more pronounced for smaller expansion coefficients. For example, for  $\Theta = 3$  the estimate of the velocity increase ( $U_m/u_f - 1$ ) proposed in [13] is approximately twice larger than the velocity increase obtained in numerical simulations. For larger expansion coefficients the difference is not so pronounced: for example, for  $\Theta = 10$  the estimated velocity increase is  $U_m/u_f - 1 \approx 0.4$  according to [13], while the numerically obtained value  $U_m/u_f - 1 = 0.31$ . Still in spite of some quantitative disagreement with the obtained numerical results the estimate [13] predicted qualitatively correct dependence of the velocity of a curved stationary flame front upon the expansion coefficient.

The influence of viscosity on the velocity of a curved flame front was also investigated. All results reported above were obtained for the Prandtl number  $Pr = 0.3$ . Numerical simulations of the dynamics of a curved flame front propagating in a fuel of different viscosity ( $Pr = 0.1, 0.3, 1$ ) were performed for the expansion coefficient  $\Theta = 5$  and the tube width  $D = \lambda_c$ . The simulations showed that velocities of the curved stationary flame fronts are independent of viscosity. The last result can be anticipated if one takes into account that the perturbation growth on the linear stage of the LD instability is independent of viscosity [9,32].

## VI. CURVED FLAMES PROPAGATING UPWARDS: THE EFFECT OF GRAVITY

Propagation of a low speed flame in tubes can be affected by gravity. It is well known that gravity plays a stabilizing role for downward propagating flames and it is destabilizing for upwards propagating flames [1,5,7,32–36]. If the gravity acceleration is directed opposite to the flame velocity, than the cold fresh fuel of higher density is supported by the combustion products of lower density, so that the condition for the Rayleigh-Taylor (RT) instability to develop at the flame front is fulfilled. For the upward propagating flames the RT instability at the flame front amplifies the effect of the LD instability. The value of the dimensionless acceleration  $\gamma = gL/u_f^2$  shows the relative contribution of the RT and LD instabilities to the perturbation growth rate for upward propagating flames [32,35]. In Fig. 9 the instability growth

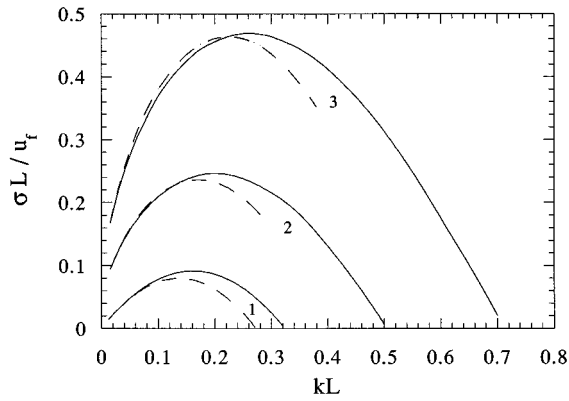


FIG. 9. The scaled instability growth rate of an upward propagating flame with the expansion coefficient  $\Theta = 5$  vs the dimensionless wave number  $kL$ . The curves 1, 2, 3 correspond to the dimensionless accelerations  $gL/u_f^2 = 0, 1, 3$ . The dashed lines show the instability growth rate calculated from Eq. (32).

rates for the case of an upward propagating flame of the expansion coefficient  $\Theta = 5$  are shown for different values of the dimensionless acceleration  $\gamma = 0; 1; 3$ . One can see that an increase of the dimensionless acceleration results in an increase of the instability growth rate and extension of the interval of possible unstable perturbations. Particularly for the upward propagating flames the cutoff wavelength  $\lambda_{cg}$  is diminished in comparison with  $\lambda_c$  for the case of zero gravity determined by Eq. (3). The shape of the dispersion curve changes as well. Unlike the case of zero gravity the wavelength of the fastest perturbations for an upward propagating flame is larger than the doubled cutoff wavelength. For this reason one may expect stronger interaction of modes on the nonlinear stage of the instability. For long wavelength perturbations the instability growth rate of the flame front can be estimated by the analytical formula [35]

$$\sigma = \sigma_0 - \frac{1}{2}kL \frac{\Theta u_f k}{(\Theta + 1)\sigma_0 + \Theta u_f k} \left[ \frac{2\Theta \ln \Theta}{\Theta - 1} \sigma_0 + \left( \frac{\Theta + 1}{\Theta - 1} \Theta \ln \Theta + \Theta - 1 \right) u_f k \right], \quad (32)$$

where  $\sigma_0$  is the instability growth rate of an infinitely thin flame propagating upwards:

$$\sigma_0 = \left( \frac{\Theta - 1}{\Theta + 1} gk + \frac{\Theta^2 + \Theta - 1}{(\Theta + 1)^2} \Theta u_f^2 k^2 \right)^{1/2} - \frac{\Theta}{\Theta + 1} u_f k. \quad (33)$$

In the case of zero gravity Eq. (32) goes over to the dispersion relation for a freely propagating flame Eq. (1). As is seen from Fig. 9, the analytical formula Eq. (32) provides a very good approximation of the instability growth rate for long wavelength perturbations up to the fastest perturbations of maximal growth rate. For a sufficiently long perturbation wavelength or for a large acceleration  $gL/u_f^2 \gg 1$  the gravity dominates and the instability growth rate coincides with the classical expression for the growth rate of the RT instability at the interface separating two incompressible fluids with the densities ratio  $\Theta$

$$\sigma_{RT} = \left( \frac{\Theta - 1}{\Theta + 1} gk \right)^{1/2}. \quad (34)$$

Similar to the linear stage of the hydrodynamic instability of an upward propagating flame, one may expect that for the case of a large acceleration and a wide tube  $gD/u_f^2 \gg 1$  the flame dynamics in tubes resembles in a sense the nonlinear stage of the RT instability in the classical configuration. The interesting point is that even in the case of a small acceleration ( $\gamma \ll 1$ ) the RT instability can strongly influence the flame propagation in a tube if the tube is sufficiently wide. The nonlinear stage of the RT instability in the classical configuration may be described as the stationary rising bubbles of the light matter and falling spikes of the heavy matter. In the two-dimensional case an open bubble in a tube of width  $D$  with ideally slippery walls rises with the velocity [37]

$$u_{RT} = \alpha \left( \frac{\Theta - 1}{\Theta + 1} 2gD \right)^{1/2}, \quad (35)$$

where the coefficient  $\alpha$  has been estimated as  $\alpha = 0.2 - 0.3$ .

When the RT instability develops at a flame front the configuration of falling spikes is no longer possible. The flame front consumes the falling fuel — the so called “fire polishing” effect happens. The numerical simulations show that in the case of a flame in tubes of moderate width the competition of the bubble formation and the fire polishing effect results in a curved stationary shape of the flame front. The flame shape is similar to the shape of a flame in the absence of gravity, but with larger amplitude and larger front curvature. The shapes of the curved stationary flames are shown in Fig. 10 for a flame with the expansion coefficient  $\Theta = 5$  propagating in a tube of width  $D = \lambda_c$  for the dimensionless gravitational accelerations  $\gamma = 0, 1, 3$ . The curvature and the length of the flame front increase with the increase of the gravitational acceleration. Because of the strong correlation of the flame velocity and the length of the flame front, discussed in the preceding section, a larger gravitational acceleration leads to the larger velocities of curved upward propagating flames. The velocity of a curved flame with the expansion coefficient  $\Theta = 5$  propagating upwards in a tube of width  $D = \lambda_c$  is shown in Fig. 11 versus the dimensionless gravitational acceleration  $\gamma = gL/u_f^2$ . The effect of the velocity increase of the curved flames propagating upwards can be described as a combined action of the LD and RT instabilities in the form of a simple analytical formula

$$u_w = \sqrt{u_{LD}^2 + u_{RT}^2} = \left( u_{LD}^2 + 2\alpha^2 \frac{\Theta - 1}{\Theta + 1} gD \right)^{1/2}, \quad (36)$$

where  $\alpha = 0.27$  and  $u_{LD}$  is the velocity of the curved flame for the case of zero gravity. The empirical formula (36) combines the effects of flame propagation and the bubble rising. As is seen from Eq. (36) the relative influence of the RT instability on the flame shape is determined by the dimensionless parameter  $gD/u_f^2$ . Still we would like to emphasize, that even for quite large values of  $gD/u_f^2$  the relative increase of the flame velocity is rather moderate, see Fig. 11. For example, for  $gD/u_f^2 = 60$  ( $\gamma = 3$ ,  $D = \lambda_c$ ) the velocity increases only by the factor 2.64. The weak effect of gravity

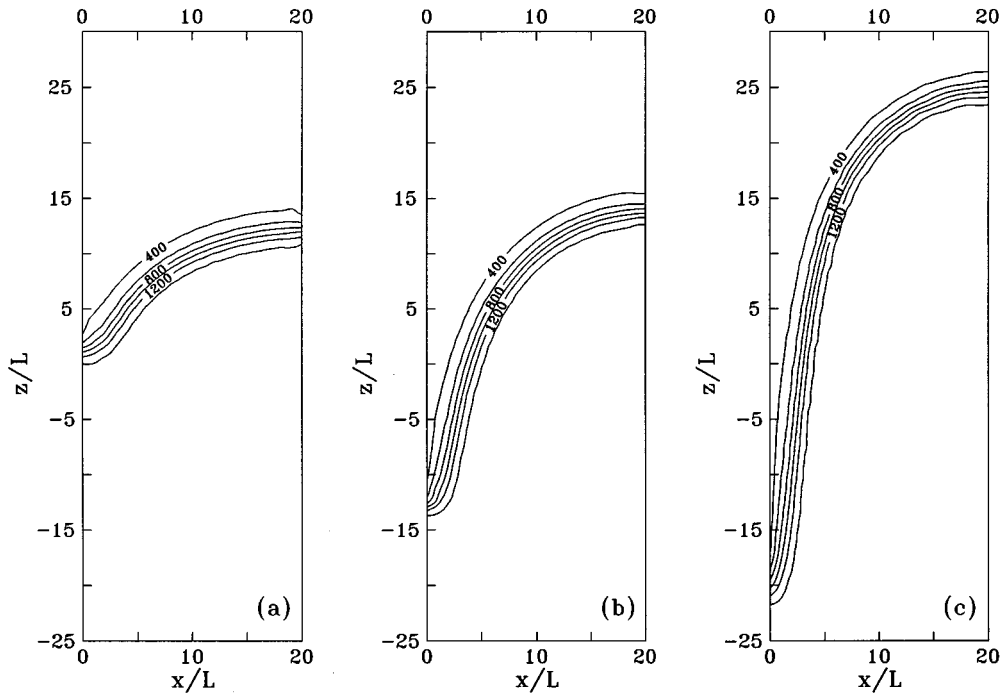


FIG. 10. The isotherms (temperature is given in K) of the curved stationary flames with the expansion coefficient  $\Theta=5$  propagating upwards in a tube of width  $D=\lambda_c$  for the dimensionless accelerations (a)  $gL/u_f^2=0$ , (b)  $gL/u_f^2=1$ , (c)  $gL/u_f^2=3$ .

may be attributed to the small numerical factor  $\alpha^2$  which appears in the theory of bubble motion, see Eq. (35).

Unlike the flames without gravity, the velocity of a curved flame propagating upwards in tubes increases with the increase of the tube width even for  $D > \lambda_c$ . Dependence of the flame velocity on the inverse tube width is shown in Fig. 12 for a curved flame with the expansion coefficient  $\Theta=5$  propagating in a gravitational field with the dimensionless accelerations  $\gamma=0;0.1;1$ . The effect of gravity is especially interesting in the case of a small dimensionless acceleration  $\gamma=0.1$ . For the tubes of moderate width  $D < \lambda_c$  the flame velocities in the cases of zero and small accelerations are quite close. However, for wider tubes  $D > \lambda_c$  the increase of the flame velocity for the upward propagating flames is considerably larger even for the case of a small acceleration  $\gamma=0.1$ . For the case of a large acceleration  $\gamma=1$  the difference between the cases of zero and nonzero gravity becomes much more pronounced. As is seen from Fig. 12, the configuration of a curved upward propagating flame is possible for much narrower tubes compared to the case of zero gravity  $\lambda_c/2 > D > \lambda_{cg}/2$ . For sufficiently narrow tubes the growth rate of both the RT and LD instabilities is strongly reduced or even suppressed by thermal conduction, see Fig. 9. For such tubes the shape of a curved flame differs only slightly from a planar one and the flame velocity is close to the velocity of a planar flame front. For slightly curved flames the similarity between the flame dynamics and the ‘‘bubble’’ rising breaks down. For this reason Eq. (36) is not applicable for flames in narrow tubes, when the hydrodynamic instabilities are almost suppressed by thermal conduction, see Fig. 12. At the same time Figs. 11, 12 demonstrate that for wider tubes the analytical formula Eq. (36) provides a very good approximation of the velocity of an upward propagating flame.

An important conclusion follows from Fig. 11 and Eq. (36) that the effect of terrestrial gravity on the upward propagating flames is much weaker than is usually assumed [38]. For example, for the experimental installation used in [34] with the tube radius  $R=2.5$  cm the gravity is much more important than the LD instability only for very slow flames with the velocities less than 20 cm/s such as the flame in the mixture 6%  $\text{CH}_4 + \text{Air}$ . On the contrary, the effect of gravity is expected to be small even for flames of the moderate velocities, like a flame in the mixture 7.7%  $\text{C}_2\text{H}_4\text{O} + \text{Air}$  ( $u_f=70$  cm/s). Finally, for the case of fast hydrogen-oxygen flames with the velocities up to 1000 cm/s the influence of gravity on the flame velocity is negligible (less than 0.1%). Unlike the laboratory flames the effect of gravity is critical for flames in astrophysics, such as the thermonuclear reaction front in Supernova events [36,39–42].

## VII. DISCUSSION

In the present paper we studied formation and stationary propagation of curved flames in tubes. The maximal velocity of a curved stationary flame in the absence of gravity is obtained for the flame propagating in a tube of width  $\lambda_c$  which allows the growth of the fastest perturbations on the linear stage of the LD instability. The analytical formula for the velocity of a curved flame is proposed. One of the important results of the simulations is that development of the LD instability on the length scales comparable to the cutoff wavelength leads to a moderate increase of the flame velocity. The velocity is not doubled as was expected earlier on the basis of the study of model equations see, for example, [14]. Even for the flames with a large expansion coefficient  $\Theta=10$  the flame velocity increases only by 30%. A much larger increase of the flame velocity is expected for a flame

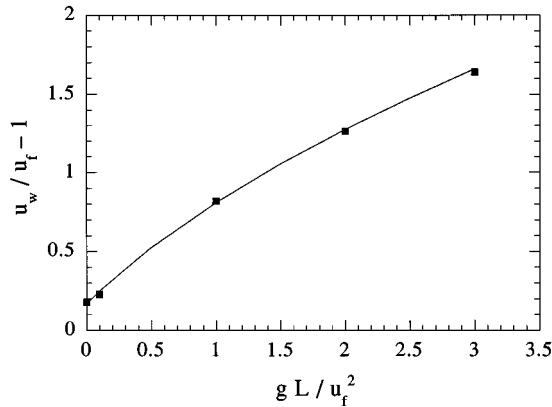


FIG. 11. The scaled velocity of a curved stationary flame  $u_w/u_f - 1$  with the expansion coefficient  $\Theta = 5$  propagating upwards in a tube of width  $D = \lambda_c$  vs the dimensionless acceleration  $gL/u_f^2$ . The markers correspond to the results of the numerical simulation, the solid line shows the fit of the flame velocity by the analytical formula Eq. (36).

front with a well pronounced fractal structure [15,18], when the LD instability develops on a length scale exceeding the cutoff wavelength by several orders of magnitude. In this sense the flame cells obtained in the present numerical simulations may be considered as the first step in the cascade of cells of different sizes expected for a fractal flame [18].

The configuration of a curved flame propagating upwards in a gravitational field was investigated as well. It was obtained that gravity leads to an additional increase of the flame velocity due to the effect of the rising of the light ‘‘bubble’’ of burning products inherent to the nonlinear stage of the RT instability. For the case of slow flames and wide tubes the RT instability becomes the most important effect, which determines the velocity of a curved flame. The analytical formula for the velocity of an upward propagating flame is proposed, which combines the effects of the bubble rising and the flame propagation. Still it is shown that the

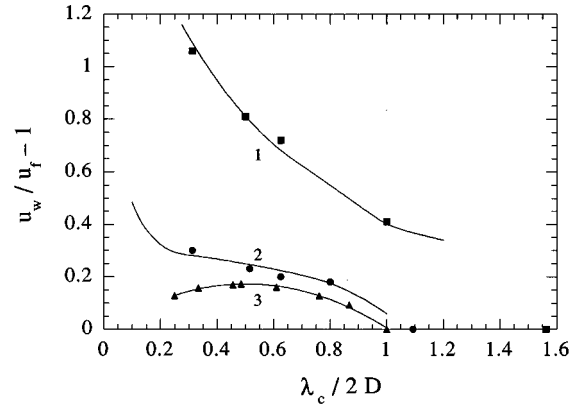


FIG. 12. The scaled velocity of a curved stationary flame  $u_w/u_f - 1$  with the expansion coefficient  $\Theta = 5$  propagating upwards vs the inverse tube width  $\lambda_c/2D$ . The markers show the results of 2D simulations and the solid lines show the estimate of the flame velocity according to Eq. (36) for the dimensionless accelerations  $\gamma = gL/u_f^2$ . Curve 1 and the filled squares correspond to  $\gamma = 1$ , curve 2 and the filled circles correspond to  $\gamma = 0.1$ , curve 3 and the filled triangles correspond to  $\gamma = 0$ .

influence of gravity on the flame velocity is much less important than was generally believed.

In the present paper we studied the dynamics of curved flames in the two-dimensional case, however, a real physical situation is, as usual, three dimensional. It is expected that the three-dimensional geometry leads to an additional increase of the flame velocity, both for the cases of zero and nonzero gravity.

#### ACKNOWLEDGMENTS

This work was supported in part by the Swedish National Board for Industrial and Technical Development (NUTEK), Grant P2204-1, in part by the Swedish Natural Science Research Council (NFR), Grant No. F-AA/Fu 10297-307, and by the Swedish Royal Academy of Sciences.

- 
- [1] Ya. B. Zel'dovich, G. I. Barenblatt, V. B. Librovich, and G. M. Makhviladze, *The Mathematical Theory of Combustion and Explosion* (Consultants Bureau, New York, 1985).
- [2] K. I. Shelkin, *Zh. Eksp. Teor. Fiz.* **10**, 823 (1940).
- [3] M. S. Uberoi, *Phys. Fluids* **2**, 72 (1959).
- [4] T. Maxworthy, *Phys. Fluids* **5**, 407 (1962).
- [5] L. D. Landau and E. M. Lifshitz, *Fluid Mechanics* (Pergamon, Oxford, 1987).
- [6] L. D. Landau, *Zh. Eksp. Teor. Fiz.* **14**, 240 (1944).
- [7] P. Pelce and P. Clavin, *J. Fluid Mech.* **124**, 219 (1982).
- [8] M. Matalon and B. J. Matkowsky, *J. Fluid Mech.* **124**, 239 (1982).
- [9] M. L. Frankel and G. I. Sivashinsky, *Comb. Sci. Technol.* **29**, 207 (1982).
- [10] M. A. Liberman, V. V. Bychkov, S. M. Golberg, and D. L. Book, *Phys. Rev. E* **49**, 445 (1994).
- [11] Ya. B. Zel'dovich, *Prikl. Mekh. Tekh. Fiz.* **1**, 102 (1966).
- [12] G. I. Sivashinsky, *Acta Astronaut.* **4**, 1177 (1977); *Annu. Rev. Fluid. Mech.* **15**, 179 (1983).
- [13] Ya. B. Zel'dovich, A. G. Istratov, N. I. Kidin, and V. B. Librovich, *Comb. Sci. Tech.* **24**, 1 (1980).
- [14] S. Gutman and G. I. Sivashinsky, *Physica D* **43**, 129 (1990).
- [15] Y. A. Gostintsev, A. G. Istratov, and Y. V. Shulenin, *Comb. Expl. Shock Waves* **24**, 70 (1988).
- [16] L. Filiand, G. I. Sivashinsky, and M. L. Frankel, *Physica D* **72**, 110 (1994).
- [17] S. I. Blinnikov and P. V. Sasorov, *Phys. Rev. E* **53**, 4827 (1996).
- [18] V. V. Bychkov and M. A. Liberman, *Phys. Rev. Lett.* **76**, 2814 (1996).
- [19] O. Thual, U. Frish, and M. Henon, *J. Phys.* **46**, 1485 (1985).
- [20] M. Gonzalez, R. Borghi, and A. Saouab, *Comb. Flame* **88**, 201 (1992).
- [21] J. C. Niemeyer and W. Hillebrandt, *Astrophys. J.* **452**, 779 (1995).

- [22] B. Denet and P. Haldenwang, *Comb. Sci. Tech.* **104**, 143 (1995).
- [23] S. Kadowaki, *Comb. Sci. Tech.* **107**, 181 (1995).
- [24] D. Dutoya and P. J. Michard, *Rech. Aérospat.* **2**, 123 (1980).
- [25] F. Dupoirieux and D. Dutoya, *Rech., Aérospat.* **6**, 15 (1987).
- [26] L. E. Eriksson, *Comp. Meth. Appl. Mech. Eng.* **64**, 95 (1987).
- [27] L. E. Eriksson, Volvo Aero Corporation Report No. 9970-1162, 1995 (unpublished).
- [28] L. E. Eriksson, Volvo Aero Corporation Report No. 9370-154, 1990 (unpublished).
- [29] E. S. Oran and J. H. Gardner, *Prog. Energy Comb. Sci.* **11**, 253 (1985).
- [30] E. S. Oran and J. P. Boris, *Numerical Simulation of Reactive Flow* (Elsevier, New York, 1987).
- [31] S. Karhi, *AIAA J.* **30**, 1220 (1992).
- [32] M. A. Liberman, V. V. Bychkov, and S. M. Golberg, *Zh. Eksp. Teor. Fiz.* **104**, 2685 (1993) [*Sov. Phys. JETP* **77**, 227 (1993)].
- [33] P. Pelce, *J. Phys.* **46**, 503 (1985).
- [34] C. Pelce-Savornin, J. Quinard, and G. Searby, *Comb. Sci. Tech.* **58**, 337, (1988).
- [35] V. V. Bychkov, S. M. Golberg, and M. A. Liberman, *Phys. Plasmas* **1**, 2976 (1994).
- [36] V. V. Bychkov and M. A. Liberman, *Astron. Astrophys.* **302**, 727 (1995).
- [37] H. Kull, *Phys. Rep.* **206**, 197 (1991).
- [38] C. K. Law and G. M. Faeth, *Prog. Energy Comb. Sci.* **20**, 66 (1994).
- [39] V. V. Bychkov and M. A. Liberman, *Astrophys. J.* **451**, 711 (1995).
- [40] V. V. Bychkov and M. A. Liberman, *Astron. Astrophys.* **304**, 440 (1995).
- [41] A. M. Khokhlov, *Astrophys. J.* **449**, 695 (1995).
- [42] D. Garcia-Senz and S. E. Woosley, *Astrophys. J.* **454**, 895 (1995).